AGB stars observed with VLTI and VLBA

VLTI/MIDI observations of oxygen-rich Mira stars

Markus Wittkowski
ESO

I. Karovicova, M. Scholz, K. Ohnaka, D. A. Boboltz

MIDI time line

• Oct 2002	Delivery to Paranal
• 15 Dec 2002	First fringes
• P73 (Apr-Sep 2004)	Offered to the community
• 8-12 April 2004	First MIDI slot for open time observations
• P76 (Oct 05-Mar 06)	MIDI/AT observations offered
	MIDI field mode and MIDI/FINITO offered
• P91 (Apr-Sep 2013)	MIDI w/ PRIMA-FSU-A; MIDI correlated flux mode

- 116 papers based on MIDI data
- ~12 on AGB stars and another ~20 on related objects (e.g., red giants, post-AGB, PNe):

  Ohnaka et al. (2005, 2007); Sacuto et al. (2007, 2008, 2013);

  Wittkowski et al. (2007); Zhao-Geisler et al. (2011, 2012);

  Karovicova et al. (2011, 2013); Klotz et al. (2012); Paladini et al. (2012)


3 Sep 2003


10 Dec 2002


3 Sep 2003

Asymptotic Giant Branch stars

- AGB stars represent the last stage of the evolution of low- to intermediate mass stars that is driven by nuclear fusion.
- The most important driver for the further evolution is mass-loss, but which is purely understood, in particular for oxygen-rich stars

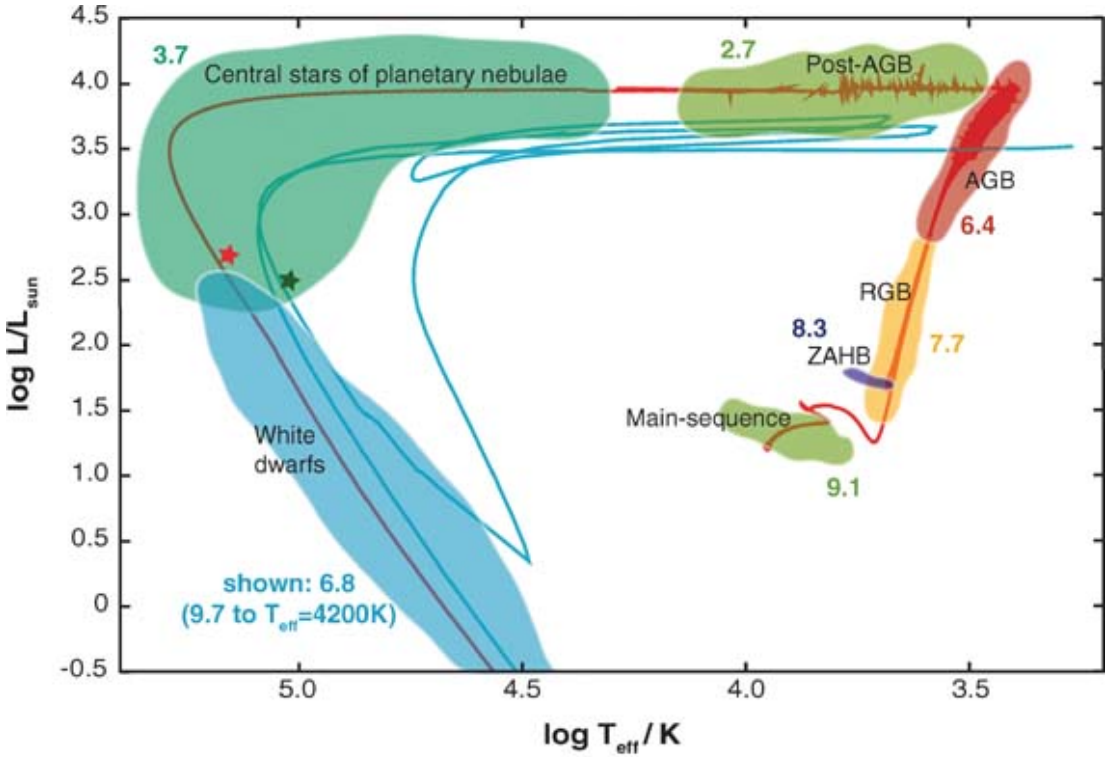

Two solar mass evolution track (Herwig 2005)

Structure of an AGB star

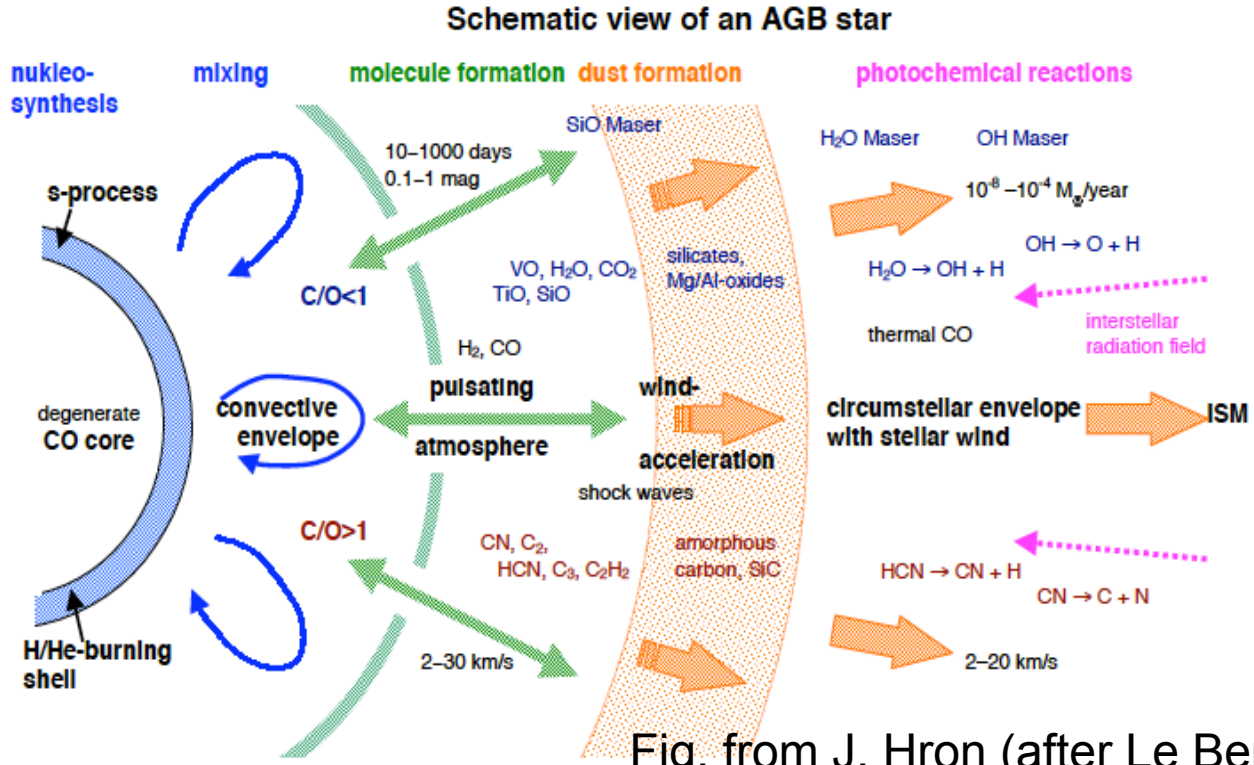

Fig. from J. Hron (after Le Bertre)

VLTI

Stellar photosphere | Molecular layers | Dust shell

ALMA

Radio photosphere

Thermal lines (e.g. SiO, CO, …)
Abundances, depletion of Si into SiO

SiO maser, high-freq. water maser

AGB stars: Current questions

- How do AGB stars loose mass, in particular in the case of oxygen-rich stars ?
- Which are the detailed differences between oxygen-rich and carbon-rich stars
- How is the mass-loss process connected to variability at different scales from pulsation (~1 year) to thermal pulses (10000 years) ?
- When and where do inhomogeneities/clumps/ asymmetries form ? Which are the shaping mechanisms ?
- Which is the role of binarity in AGB stars?
- Are mass-loss mechanisms for AGB and RSG stars similar or different?

MIDI and VLBA observations of S Ori

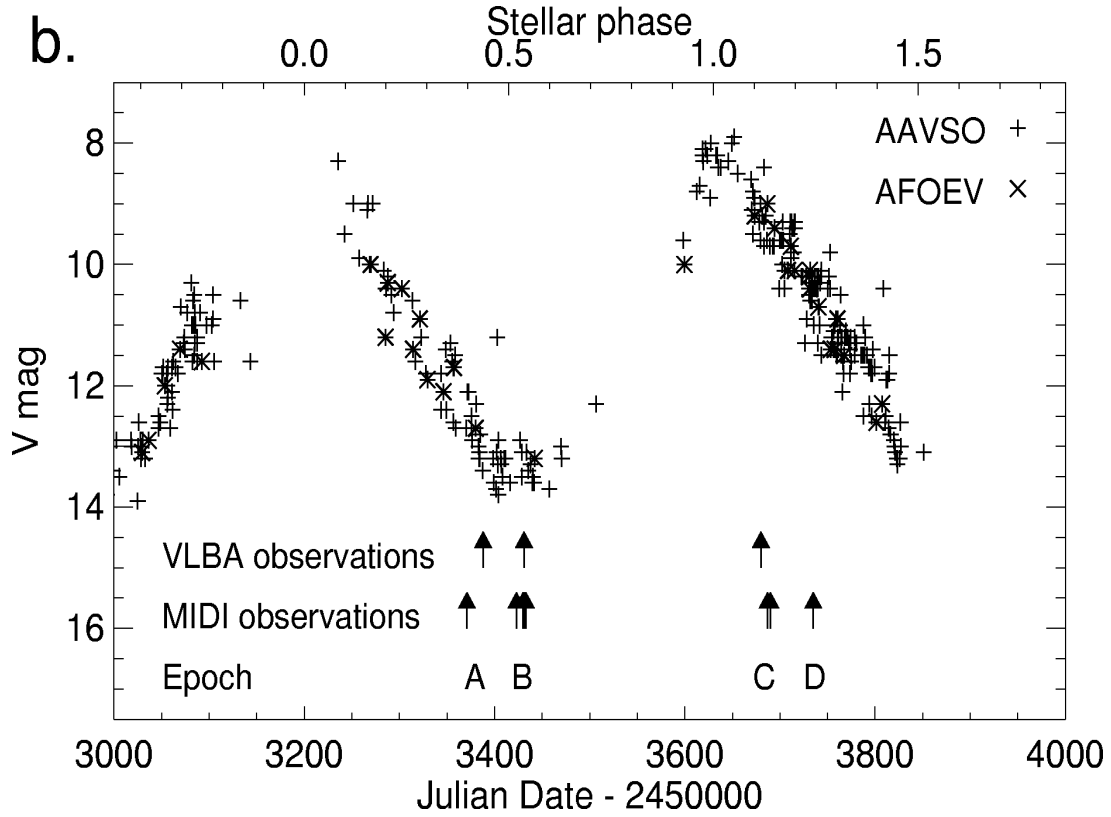

3 contemporaneous epochs between Dec 2004 and Nov. 2005 at phases 0.44, 0.56, 1.15, (1.27, MIDI only).

Wittkowski, et al. 2007

Modeling

- Photosphere and geometrically extended molecular layers (TiO, SiO, H_2O, CO): Self-excited dynamic model atmospheres by Ireland, Scholz, & Wood (2004a), Ireland, Scholz, Tuthill, and Wood (2004b) [P/M series], Ireland, Scholz, & Wood (2008, 2011) [CODEX series].
- Dust shell: Radiative transfer model using the Monte Carlo radiative transfer code mcsim_mpi by Ohnaka et al. (2006). Following Lorenz-Martins & Pompeia (2000), we use Al_2O_3 (Koike 1995; Begemann 1997) and/or silicate (Ossenkopf 1992) grains with different inner radii. Dynamic model atmospheres used as inner source.
- Maser emission: Combination of the dynamic model atmosphere and dust shell model (P/M series) with a maser propagation model of the SiO maser emission (Gray et al. 2009, MNRAS, 394, 51). Includes high-frequency SiO maser emission. Combination with CODEX series is work in progress.

MIDI observations of S Ori

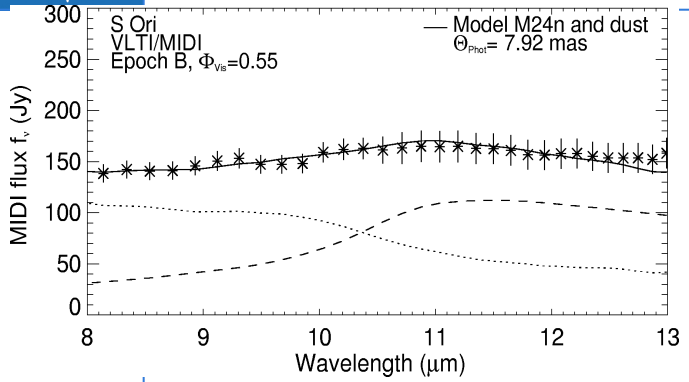

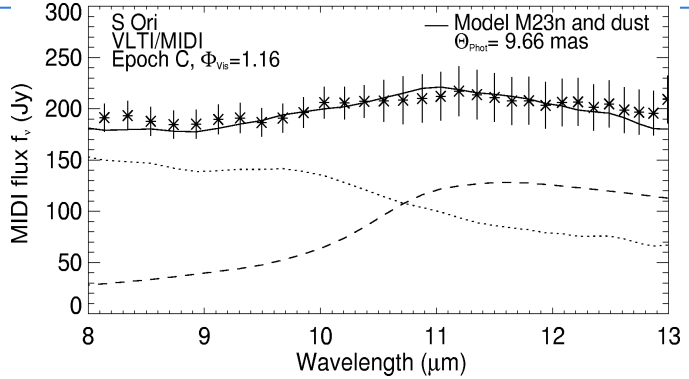

Total flux

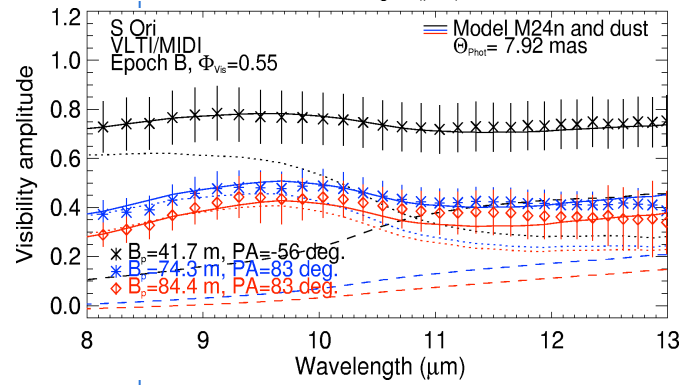

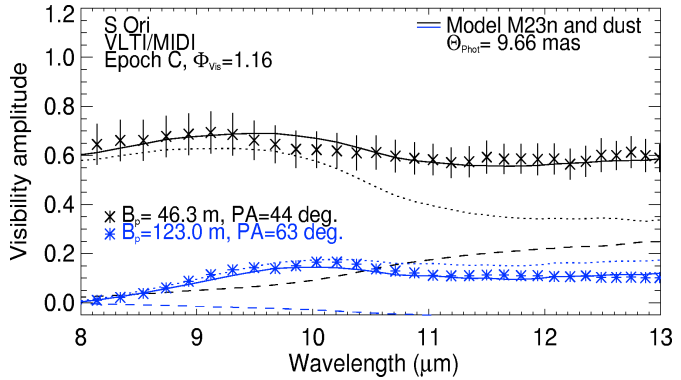

Visibility

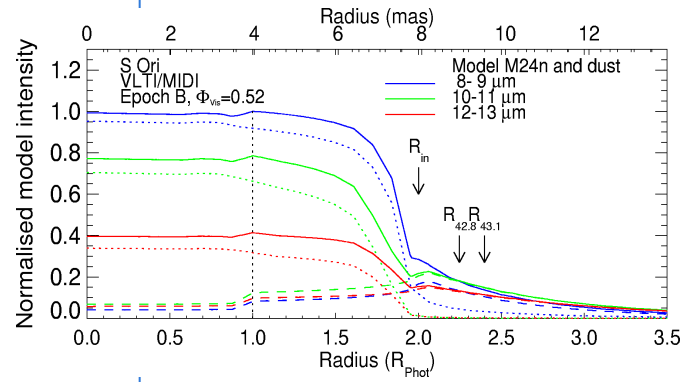

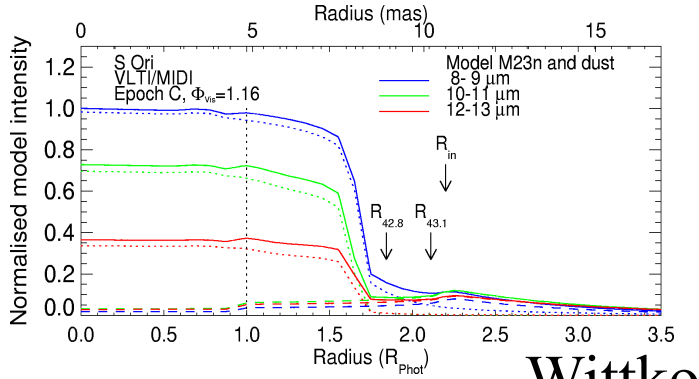

Model intensity

Wittkowski et al. 2007

VLTI/MIDI and VLBA/SiO maser observations of S Ori

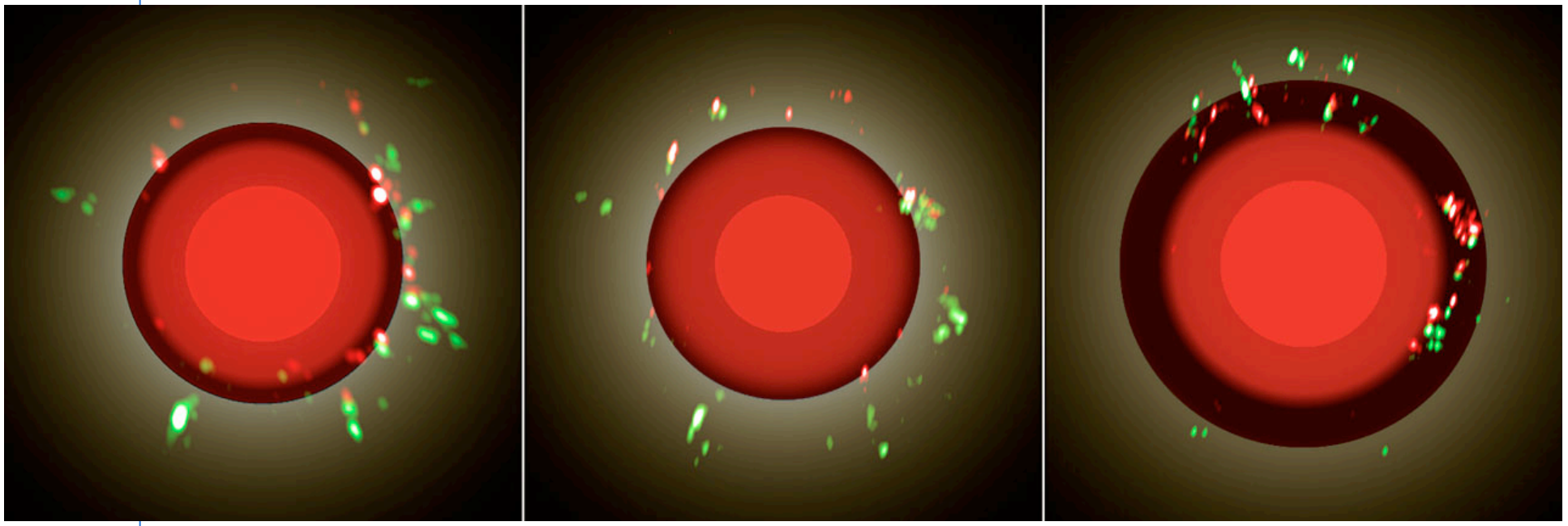

- (red) v=2, J=1-0, 42.8 GHz (green) v=1, J=1-0, 43.1 GHz maser images on MIDI model with photosphere, molecular layer, Al_2O_3 dust.
- Al_2O_3 dust has an inner radius of ~2 stellar radii, and may be co-located with the SiO maser region.
- The location of the SiO maser emission is consistent with earlier such observations and with theoretical models by Gray et al. 2009.
- The maser velocity structure indicates a radial gas expansion with velocity ~10 km/sec.

Wittkowski, et al. 2007

Maser Propagation Model

	Model Parameters					Maser Ring Radii (photospheric units)					
Model+dust	ϕ	R_{s1}	R_{s2}	R_{in}	$R_{8.13}$	$R_{43.1}$	$R_{42.8}$	$R_{v=1,J=2-1}$	$R_{v=2,J=3-2}$	$R^{obs}_{43.1}$	$R^{obs}_{42.8}$
M21n+D	0.1	1.3	2.5	2.4	1.8	1.9±0.4	1.9±0.4	2.4±0.7	2.0±0.4	-	-
M22+A	0.25	1.6	2.6	1.8	1.6	1.9±0.3	1.8±0.3	1.8±0.5	1.8±0.3	2.2±0.3	2.1±0.2
M23n+C	0.3	1.7	2.8	2.2	1.7	1.9±0.2	1.8±0.2	1.9±0.2	1.9±0.2	2.1±0.3	1.9±0.2
M24n+B	0.4	2.0	-	2.0	2.0	2.1±0.5	2.4±0.4	-	-	2.4±0.3	2.3±0.4

- Modeled masers form in rings with radii between 1.8 – 2.4 R_{Phot}, consistent with our S Ori VLBA observations, with other observations, and with earlier models.
- New models confirm the *v*=1 ring at larger radii than the *v*=2 ring.
- Al_2O_3 dust, located close to the SiO maser region, can both suppress and enhance maser emission.
- Maser rings, a shock front, and the 8.13 mu layer appear to be closely related, suggesting that collisional and radiative pumping are closely related spatially, and therefore temporally.
- Maser variability and number of spots may not be consistent with observations
  because of re-setting of masers in the model at each phase.

Gray et al. 2009

MIDI observations of RR Aql

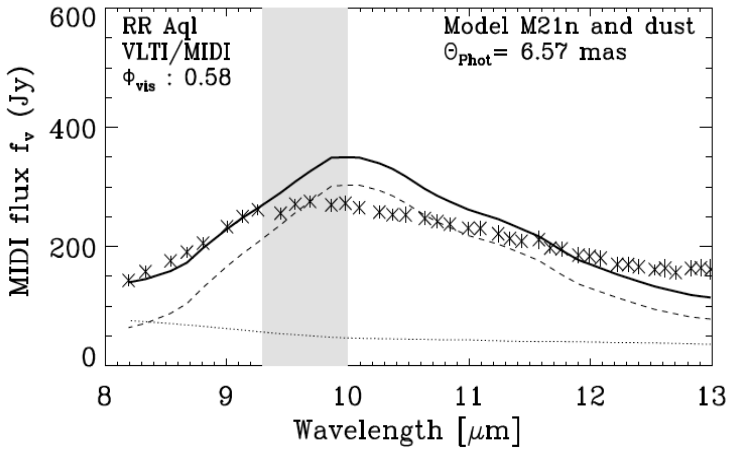

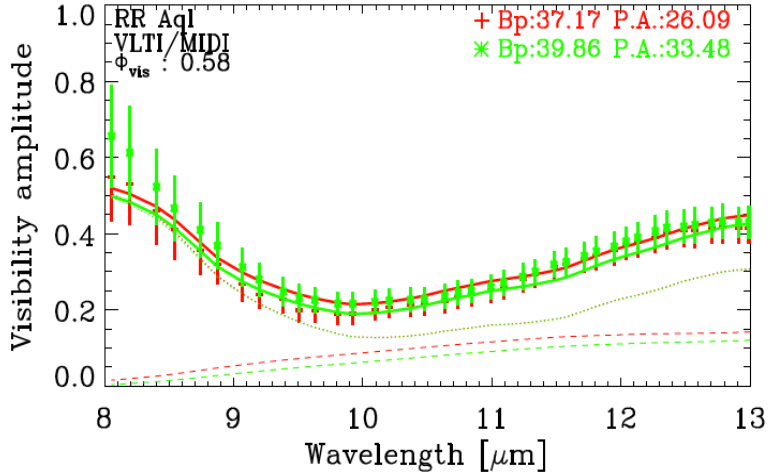

Model	τ_V (Al_2O_3)	τ_V (silicate)	R_{in}/R_{Phot} (silicate)	p (silicate)	Θ_{Phot} [mas]
M21n	0.0	2.8 ± 0.8	4.1 ± 0.7	2.6 ± 0.3	7.6 ± 0.6

- Modeling approach of a silicate dust shell is well consistent with our data.
- No detection of intra-cycle and cycle-to-cycle variability of the dust shell within our uncertainties; consistent with our modeling approach
- MIDI data are not sensitive to an additional Al_2O_3 dust shell with relatively low optical depth.

Karovicova et al. 2011

MIDI intracycle variations ?

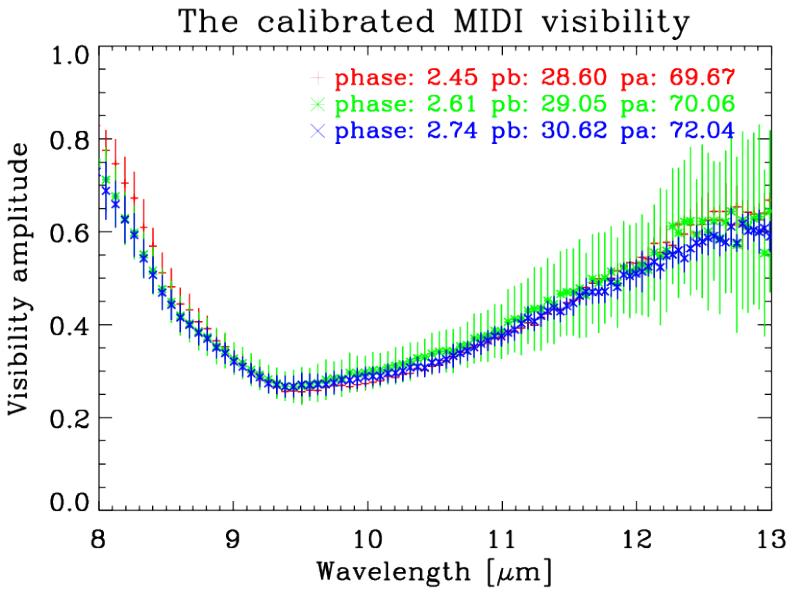

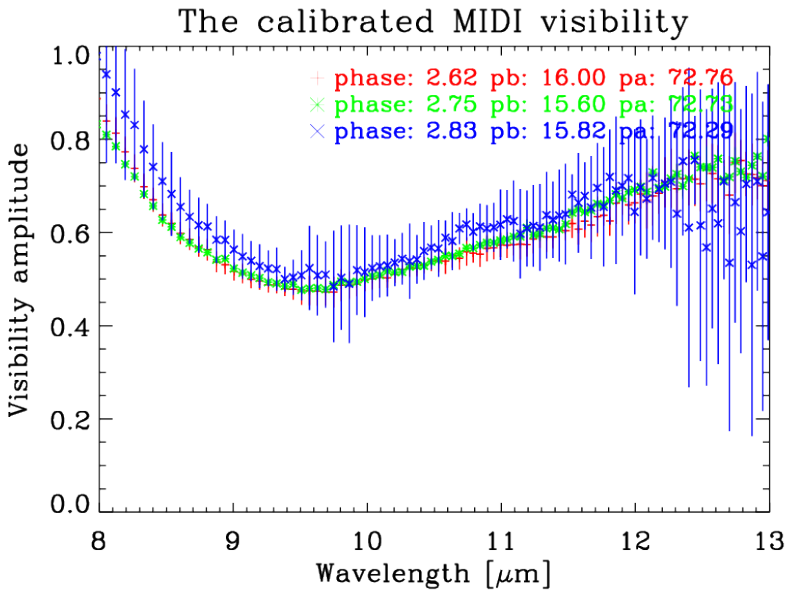

pulsation phase :	**2.45**	**2.61**	**2.74**
projected baseline :	**28.60**	**29.05**	**30.62**
position angle :	**69.67**	**70.06**	**72.04**

pulsation phase :	**2.62**	**2.75**	**2.83**
projected baseline :	**16.00**	**15.60**	**15.82**
position angle :	**72.76**	**72.78**	**72.29**

NO intra-cycle visibility variations

Karovicova et al., 2011

MIDI cycle to cycle variations ?

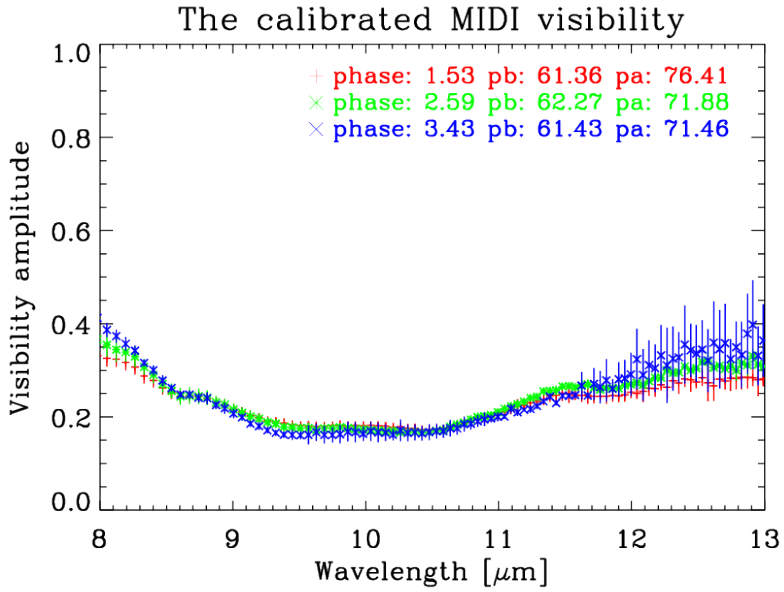

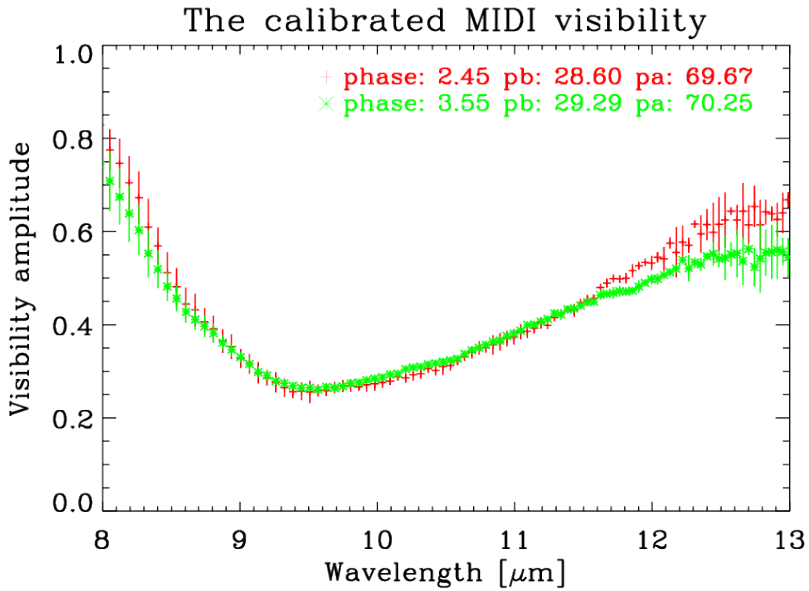

pulsation phase :	**1.53**	**2.59**	**3.43**
projected baseline :	**61.36**	**62.27**	**61.43**
position angle :	**76.41**	**71.88**	**71.46**

pulsation phase :	**2.45**	**3.55**
projected baseline :	**28.60**	**29.29**
position angle :	**69.67**	**70.25**

NO cycle to cycle visibility variations

Karovicova et al., 2011

Dust condensation sequence

- Additional targets (S Ori, R Cnc, GX Mon) processed in the same way:
- Al_2O_3 dust confirmed with an inner radius of ~ 2 photospheric radii; silicate dust with an inner radius of ~4 photospheric radii.
- Modeled dust temperatures at the inner radii are consistent with dust condensation temperatures of Al_2O_3 (~1400 K) and warm silicates (~1000 K)

		Mass-loss rate	τ_V	R_{in}/R_{Phot}
R Cnc	Al_2O_3 dust	0.2 10^{-7} M_{sun}/yr	1.4	2.2
S Ori	Al_2O_3 dust	2.2	1.5	1.9
RR Aql	Silicate dust	9.1	2.8	4.1
GX Mon	Al_2O_3 + Silicate dust	54	1.9 / 3.2	2.1 / 4.6

- Dust content of stars with low mass-loss rates dominated by Al_2O_3, while dust content of stars with higher mass-loss rates predominantly exhibit significant amount of silicates, as suggested by Little-Marenin & Little (1990), Blommert et al. (2006).

Karovicova et al. 2013

Aluminum number densities

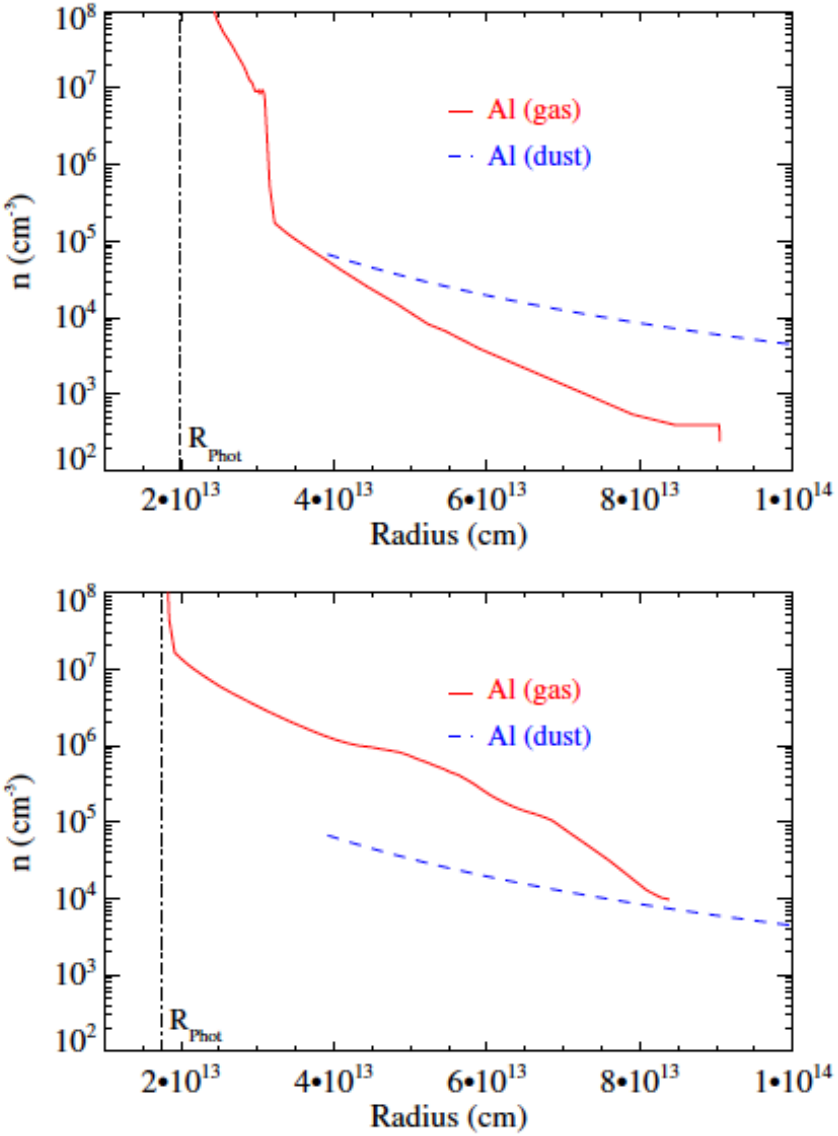

- In a sufficiently extended atmosphere, the number density of aluminum can match that of the best-fit dust shell near the inner radius, up to the condensation radius of warm silicates
- Al_2O_3 can be seed particles for the further dust formation
- Stars with low mass-loss rates form dust that preserves the spectral properties of Al_2O_3 . Stars with high mass-loss rates form dust with properties of warm silicates.

Seed particles and dust condensation

- Titanium and aluminum oxides: Dust formation starts with TiO clusters, which can serve as growth centers for both Al_2O_3 and silicates (Gail & Sedlmayer 1999). Al_2O_3 can also condense on its own with condensation temperatures around 1400 K. Al_2O_3 grains may become coated with silicates at larger radii and can serve as seed nuclei for the subsequent silicate formation (e.g. Deguchi 1980, and others).

- Heteromolecular condensation of iron-free magnesium-rich (forsterite) silicates based on Mg, SiO, H_2O (Goumans & Bromley 2012). Such grains may exist at small radii (1.5 ..2 R_*) (Ireland et al. 2005, Norris et al. 2012). Micron-sized grains may drive the wind (Höfner 2008).

- SiO cluster formation as seeds for silicate dust formation. SiO cluster formation thought to take place at temperatures below 600 K; New measurements indicate higher SiO condensation temperatures, and may be compatible with dust temperatures around 1000 K (Gail et al. 2013).

AMBER spectro-interferometry of red giants and supergiants

Atmospheric molecular layers of H_2O and CO are a common phenomenon of evolved oxygen-rich stars of different luminosities and mass-loss rates

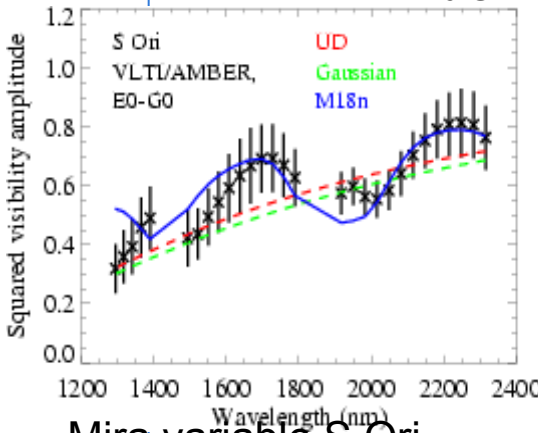

Mira variable S Ori
Wittkowski et al. 2008

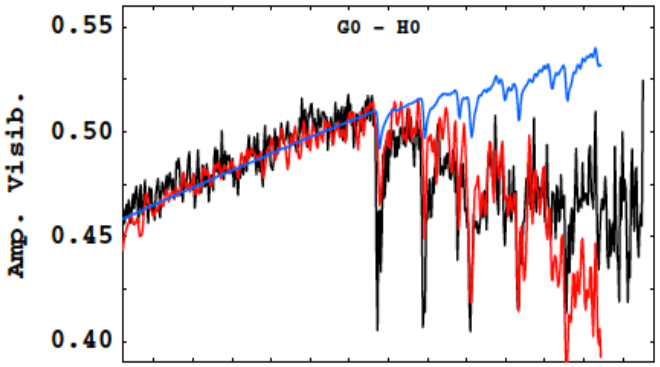

SR variable RS Cap
Marti-Vidal et al. 2010

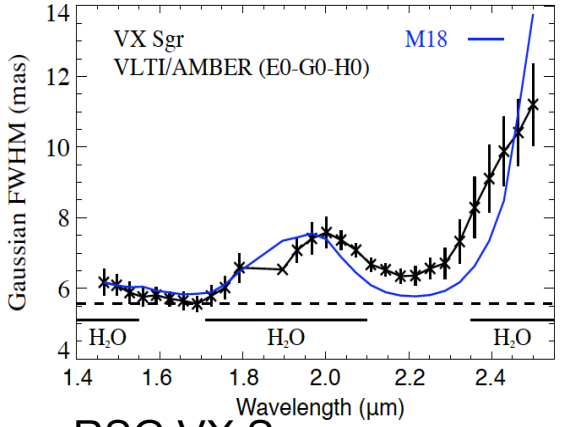

RSG VX Sgr
Chiavassa et a. 2010

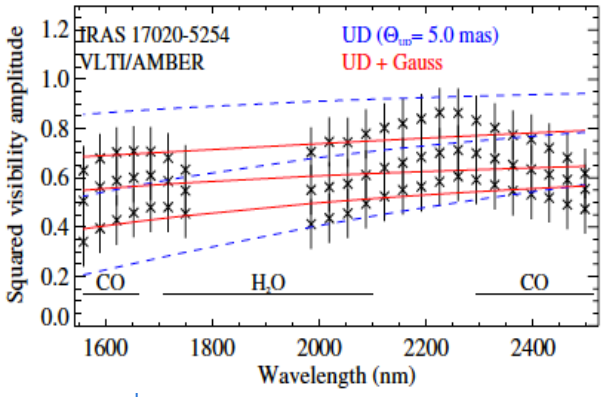

OH/IR star IRAS 17020-5254
Ruiz-Velasco et al. 2011

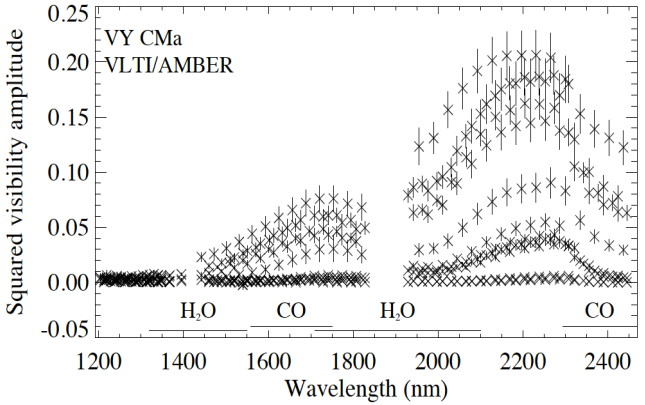

RSG VY CMa
Wittkowski et al. 2012

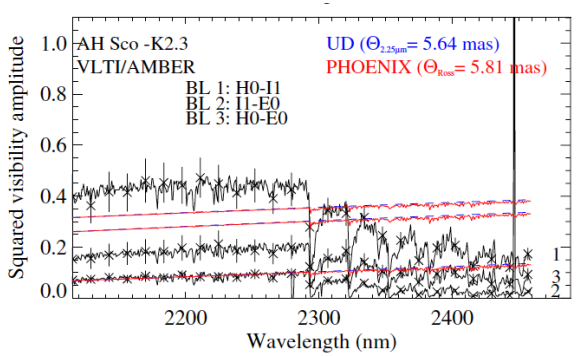

RSG AH Sco, and other RSGs
Arroyo-Torres et al., 2013

AMBER observations of R Cnc compared to CODEX dynamic model atmospheres

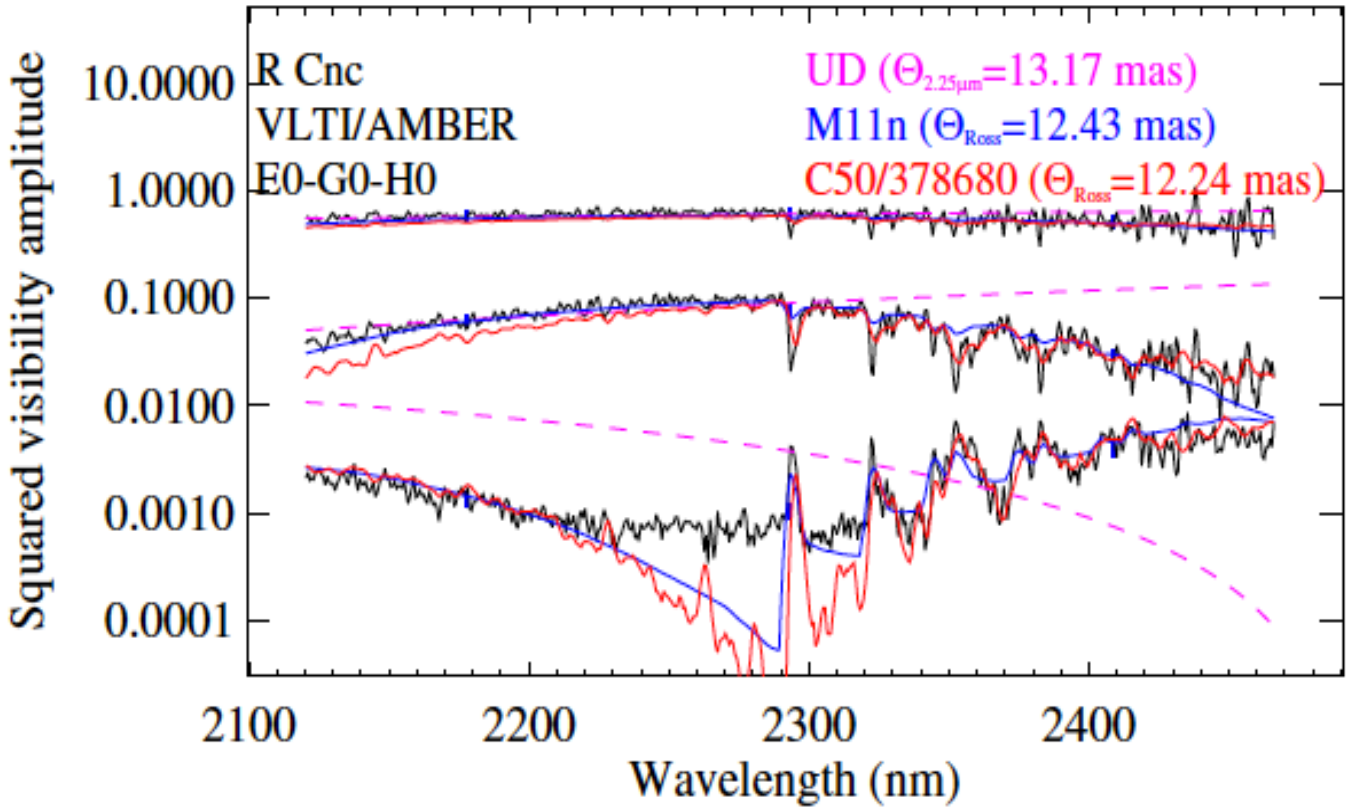

Visibilities are well consistent with predictions by CODEX dynamic model atmospheres with only small deviations.

Wittkowski et al. 2011

Asymmetries at different layers

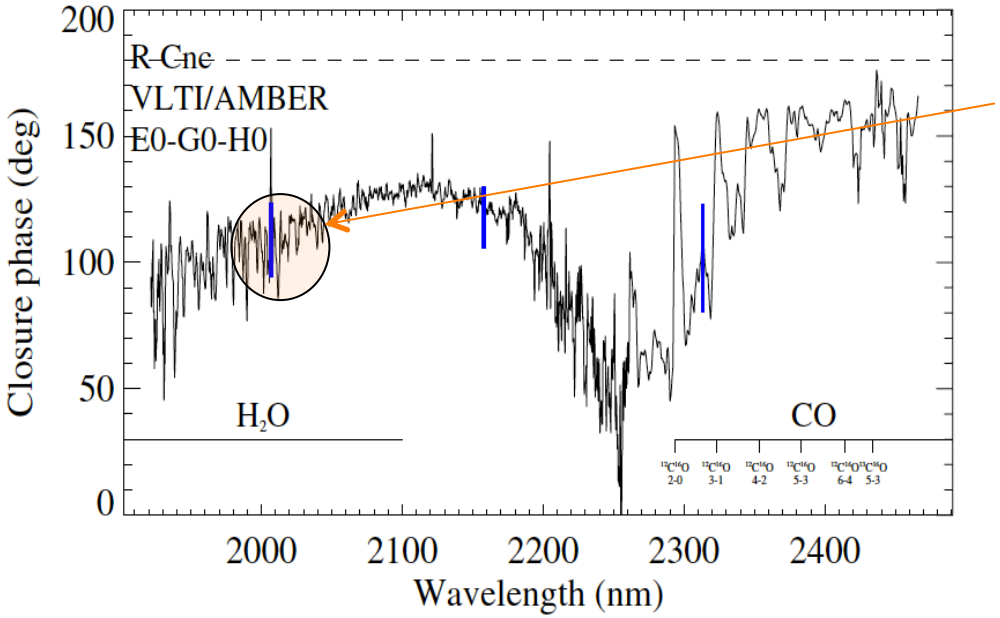

For example, one unresolved spot at separation
4 mas contributing 3% of the total flux

- Wavelength-dependent closure phases indicate deviations from point symmetry at all wavelengths and thus a complex non-spherical stratification of the atmosphere.
- Can be interpreted as a signature of large-scale inhomogeneities/clumps of molecular layers at different radii.
- These might be caused by pulsation- and shock-induced chaotic motion in the extended atmosphere as theoretically predicted by Icke et al. (1992) and Ireland et al. (2008, 2011).

Wittkowski et al. 2011

Summary

- VLTI resolves the photospheres, molecular atmospheric layers, and dust shells of AGB stars.
- Spectro-interferometry helps to isolate continuum and molecular bandpasses, and to characterize the dust grains.
- MIDI observations of oxygen-rich Mira stars indicate Al_2O_3 dust shells with inner radii of about 2 stellar radii and silicate dust shells with inner radii of about 4 stellar radii. Dust temperatures are consistent with condensation radii of these grains.
- Number densities of aluminum can be large enough in sufficiently extended atmospheres to match the number densities of Al in Al_2O_3 shells. Al_2O_3 grains can thus be seed particles for the further dust condensation.
- Stars with low mass-loss rates predominantly form dust that preserves the spectral properties of Al_2O_3. Stars with higher mass-loss rates form dust with properties of warm silicates.
- Near-infrared interferometry is consistent with predictions by latest CODEX dynamic model atmospheres with only small deviations.
- Near-infrared interferometry indicates asymmetries, possibly small-scale clumpiness, of the molecular layers.

Other topics, Outlook

- Large program by Paladini et al.
- MIDI data coordinated with AMBER imaging program (Karovicova et al.)
- Carbon-rich Miras
- SR variable AGB stars
- Comparison to Red Supergiants (cf. Arroyo-Torres et al. 2013; in prep.)
- Imaging studies to come